Pan and Yang *EURASIP Journal on Advances in Signal Processing* (2021) 2021:60
https://doi.org/10.1186/s13634-021-00772-0

EURASIP Journal on Advances in Signal Processing

RESEARCH Open Access

Downlink multi-user algorithms for millimeter-wave wideband linear arrays on PD-NOMA-based squint steering beams

Xiaoliang Pan and Luxi Yang*

*Correspondence:
lxyang@seu.edu.cn
School of Information Science and Engineering, Southeast University, 210096 Nanjing, China

Abstract

This article investigates using a phased linear antenna array instead of the planar array to circumvent the problem that two frequency squint steering main beams cannot cover any two beam directions simultaneously. First, we approximate the donut-shaped main beam of the linear array by means of multiple pencil-shaped main beams of a virtual planar array for matching the steering main beam of the linear array with the multi-path sparse scattering channel model mathematically and give a method for calculating the number of antenna elements of the virtual array. Second, we cope with possible inter-user interference on a single squint main beam of the linear array in some scenarios by means of the power-domain non-orthogonal multiple access (PD-NOMA) technique, making it possible to support communication with two users on a single squint main beam at the base station (BS) side. The feasible domain of PD-NOMA is given when a single antenna is used for both the BS and the user end, assuming a two-user successive interference cancellation (SIC) decoding power ratio limit. Third, three algorithms are given for serving multi-user at the BS via squint beams of the linear array. Finally, numerical results show that the second proposed algorithm supporting PD-NOMA pairing within a single donut-shaped squint main beam significantly increases the number of simultaneous users served within a single cellular system.

Keywords: Millimeter-wave, Wideband array, Squint beam, Power-domain NOMA

1 Introduction

Wideband millimeter-wave (mmWave) communications have received increasing attention in recent years, and the beam squint problem caused by phase differences between frequencies in the radio frequency (RF) analog domain induced by the utilization of non-ideal wideband phase shifters is one of the important problems encountered [1–3]. While the use of frequency squint multi-beam to serve multi-user within a cellular cell has been studied [3], the restricted horizontal azimuth of the squint steering beams introduced by employing the planar antenna array limits its application in cellular communications. In contrast, the steering beam of a linear array arranged in the z-axis can cover all horizontal azimuths in the x-y plane while changing the elevation angle, thus avoiding the problem

of restricted horizontal azimuth of the squint beam of a planar array. However, the hollow conical main beam of the linear array raises two new issues: (i) the matching of the donut-shaped steering main beam and the sparse scattering channel model and (ii) the handling of the additional interference from such main beams over the corresponding pencil-shaped beams of the planar array.

As for the former issue, the mmWave sparse scattering Saleh-Valenzuela channel model represents one channel path according to the form of the product of beam steering vectors of antenna arrays at both the transmitting and receiving ends [4, 5]. For linear arrays, the array factor and channel path are generally described by one angular parameter in a 2-D scenario [6], which is more convenient and concise to describe the nature of the array, but the main direction of the steer beam of a linear array is donut-shaped in 3-D space, so there may exist scattering paths at different horizontal azimuths, where the angle-of-departure (AoD) of a particular channel path is within the angular range of the transmitting donut-shaped main beam. Therefore, it is not complete to describe the channel information of a linear array in the 3-D scenario with only one angular information, which raises the problem of matching the steer beam and the channel path. To the extent of the authors' knowledge, this issue has not received sufficient attention so far.

On the latter problem, we draw on the joint spatial division and multiplexing (JSDM) grouping approach [7, 8] and the power-domain non-orthogonal multiple access (PD-NOMA) scheme [9–11] to deal with the multi-user interference between steering beams and on a donut-shaped main beam of the linear array at the base station (BS) side, respectively. On the one hand, the work in [7] assumes that the BS is high placed, leading to scatterers mainly at the user end, and therefore, the majority path of a user has a relatively close AoD, so the one-ring model is adopted to model the channel for each user. Afterwards, the users are divided into several orthogonal or near-orthogonal groups based on the channel state information, and then the interference between users is processed within the groups. Whereas the work in [8] assumes that multi-user can share a common scatterer in the mmWave cellular communication scenario, the user grouping is then performed by exploiting the channel covariance information, which can also be interpreted as a grouping by the AoD of the channel paths at the BS side.

On the other hand, the downlink PD-NOMA scheme multiplexes time-frequency blocks and mitigates interference by means of signal superposition at the BS end and successive interference cancellation (SIC) at some receivers [9]. In the mmWave cellular scenario, it is currently evolving mainly from NOMA pairing between near and far users within a single main beam to the more novel NOMA pairing among multi-beam [12]. The work in [13] investigates the beam design and power allocation problems in the two-user paired PD-NOMA scheme, without considering the effect of the donut-shaped main beam of the linear array. As the AoD of the scattering path of multi-user is potentially on a single donut-shaped main beam of the linear array at the transmitter end, in this paper, we use the PD-NOMA to enable a single squint beam of a wideband phased array at the BS end to communicate with two users simultaneously in some scenarios, further increasing the number of users served concurrently in the system. To briefly illustrate the frequency squint property of the wideband array, we only employ the steering beam and do not consider the possibility of more complex frequency squint precoding schemes, which also avoids the effect of additional non-convexity introduced into the precoding design optimization problem by the constant modulus constraint of phase shifters

in the array. In this case, the problem of finding suitable users for pairing and allocating the transmit power for the two paired users needs to be addressed in order to implement the PD-NOMA opportunity communication.

The remainder of this paper is organized as follows. In Section 2, we address the problem of matching the donut-shaped main beam of the linear array with the sparse scattering channel model in a 3-D scenario, as well as providing both the channel model and the system model. In Section 3, we first discuss NOMA user pairing strategies for a steering beam, after which three beam squint algorithms for mmWave multi-user communications are presented. In Section 4, simulation results show the performance of the proposed algorithms, before concluding the paper in Section 5.

Notation: Boldface uppercase letters, boldface lowercase letters, and lowercase letters are used to denote matrices, vectors, and scalars, respectively. The superscripts $(\cdot)^T$ and $(\cdot)^H$ denote the transpose and conjugate transpose, respectively; $\|\cdot\|_F$ represents the Frobenius norm of a matrix; $\lfloor\cdot\rceil$ denotes the rounding function; $|\cdot|$ is the amplitude of a complex value.

2 Matching of the scattering path and the steering main beam

It is assumed that the linear array is placed in the z-axis, thus having a unique elevation angle in the main direction of its steering beam, which facilitates the formulation of channel modeling and algorithm design when using the steering beam. As shown in Fig. 1, the main direction of the steering beam of the linear array is donut-shaped and can be divided into multiple pieces by vertical slicing, each piece being approximated by one steering main beam of the same virtual planar array in the x-y plane. Moreover, due to

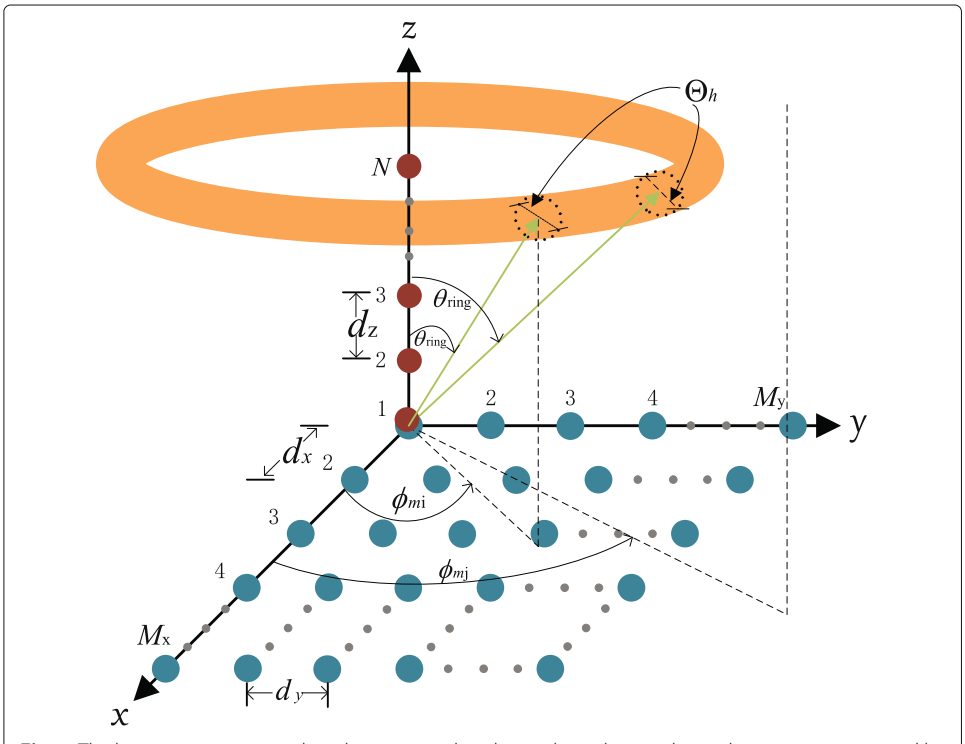

Fig. 1 The linear array is arranged on the z-axis, and its donut-shaped steered main beam is approximated by several steering beams of a virtual planar array on the x-y plane

the limitations of scatterer size in the channel and beamwidth at the transmitter side, the scattering path of the mmWave channel in practical cellular communication scenarios is more directional and can generally be described by the array response of a planar array. Accordingly, the channel path can be specified by the array response of the virtual planar array corresponding to the linear array at the BS side, which is thus mathematically coherent from the transmitter, channel, and receiver side. In addition, it is important to ensure that the power in one direction of the donut-shaped main beam is not excessive by the angular separation of the horizontal azimuth ϕ of the two adjacent slices. Furthermore, it is not necessary for this virtual ring main beam to be complete. If there is no scattering path in some horizontal azimuth range, the slices in the corresponding range can be removed to give a clearer picture of the connection between the transmitter beam and the channel scattering path. If there are multiple AoDs within the half-power beamwidth (HPBW) of the virtual planar array corresponding to the same donut-shaped main beam, the relationship to these channel paths can be represented by a slice in the main beam instead.

2.1 Number of elements in the virtual planar array

As shown in Fig. 1, the normalized array factor for a linear array of N uniformly spaced array elements placed on the z-axis and with the origin set as the reference point can be written as

$$\overline{\mathrm{AF}}_{\mathrm{Linear}} = \frac{1}{N}\sum_{n=1}^{N} e^{j(n-1)\psi}, \tag{1}$$

where

$$\psi = kd\cos\theta - \beta, \tag{2}$$

where k is the wave number, d is the array element spacing, θ is the elevation angle, and β is the phase difference of the emitted signals from adjacent array elements. After adjusting the reference point to the array midpoint [6], the array factor can be approximated as

$$\overline{\mathrm{AF}}_{\mathrm{Linear}} \approx \frac{\sin\left(\frac{N}{2}\psi\right)}{\frac{N}{2}\psi}. \tag{3}$$

In (2), by setting $\psi = 0$, we have

$$\beta = kd\cos\theta_m, \tag{4}$$

where θ_m is the elevation angle corresponding to any horizontal azimuth angle in the donut-shaped steering main beam direction of the linear array, which can be kept to a uniform value of θ_{ring} by selecting a suitable coordinate system. Since it is possible for the donut-shaped main beam to be irradiating several scatterers in the physical channel, the connection between the transmitting main beam and the channel path can be described by a set of steering main beams of a planar array with disjoint HPBW ranges when assuming that the energy radiated by the side lobes in the transmitting beam at the receiving end is highly attenuated and negligible due to atmospheric absorption of mmWave. Thus, by approximating the part of the array factor of the linear array in the first quadrant through the combination of the normalized array factors of a virtual planar array in the x-y plane

in Fig. 1, and more precisely, by approximating the main lobe of the steering beam of the linear array by the main lobes of several steering beams of the planar array and neglecting the effect of the side lobes, we have

$$\overline{\mathrm{AF}}_{\mathrm{linear}}(\theta_m) \approx \sum_{k=1}^{K} \overline{\mathrm{AF}}_{\mathrm{planar}}(\phi_{m_k}, \theta_m). \tag{5}$$

The half-power direction θ_h of the main beam of the linear array can be determined by $\overline{\mathrm{AF}} = \sqrt{0.5}$. When $\frac{\sin x}{x} = \sqrt{0.5}$, $x \approx \pm 1.391$, $x = N\psi/2$ from (3), which is substituted into (2) to give[1]

$$\theta_{hi} \approx \arccos\left[\frac{1}{kd}\left(\beta \pm \frac{2.782}{N}\right)\right]. \tag{6}$$

Therefore, the HPBW of the linear array can be approximated as

$$\Theta_h\left(f_i\right) \approx 2\left|\theta_{mi} - \theta_{hi}\right|. \tag{7}$$

On the other hand, the HPBW of a planar array in the x-y plane can be expressed as [6]

$$\Theta_h\left(f_i\right) = 1 \Bigg/ \sqrt{\cos^2\theta_{mi}\left[\Theta_{x0}^{-2}\cos^2\phi_m + \Theta_{y0}^{-2}\sin^2\phi_m\right]}, \tag{8}$$

$$\Psi_h\left(f_i\right) = 1 \Bigg/ \sqrt{\Theta_{x0}^{-2}\sin^2\phi_m + \Theta_{y0}^{-2}\cos^2\phi_m}, \tag{9}$$

where Θ_{x0} and Θ_{y0} are the HPBWs of linear arrays equally spaced on the x- and y-axes with the number of array elements M_x and M_y, respectively, with the beam direction toward the z-axis, with

$$\Theta_{x0}\left(f_i\right) \approx 2\arcsin\left(\frac{2.782c}{2\pi dM_x f_i}\right), \tag{10}$$

in which c is the velocity of electromagnetic wave. Similarly, replacing M_x with M_y in (10) gives Θ_{y0}. When a square planar array is employed, such that $M = M_x = M_y$, (8) and (9) can be further simplified to

$$\Theta_h\left(f_i\right) = \Theta_{x0}/\cos\theta_{mi}, \tag{11}$$

$$\Psi_h\left(f_i\right) = \Theta_{x0}. \tag{12}$$

To approximate the steering main beam of the linear array by steering main beams of the planar array, let (7) and (11) have equal HPBWs, which gives

$$\arccos\left(\frac{\beta}{kd} - \frac{2.782}{kdN}\right) - \theta_{mi} = \arcsin\left(\frac{2.782c}{2\pi . dMf_i}\right) \Bigg/ \cos\theta_{mi} \tag{13}$$

Since the HPBW is not perfectly symmetrical on both sides in the main beam direction, the relationship in (13) can be written exactly as

$$\arccos\left(\frac{\beta}{kd} - \frac{2.782}{kdN}\right) - \arccos\left(\frac{\beta}{kd} + \frac{2.782}{kdN}\right) = 2\arcsin\left(\frac{2.782c}{2\pi dMf_i}\right) \Bigg/ \cos\theta_{mi}. \tag{14}$$

Substituting (4) into (14) yields

[1] For convenience, in this article, we abbreviate the main direction $\theta_m\left(f_i\right)$, the half-power direction $\theta_h\left(f_i\right)$, and the grating lobe direction $\theta_{gi}\left(f_i\right)$ of the beam operating at frequency f_i as θ_{mi}, θ_{hi}, and θ_{gi}, respectively, which are further abbreviated to θ_m, θ_h, and θ_g when working at the central frequency f_c.

$$
\begin{aligned}
M &= \frac{2.782c}{2\pi f_i d} \\
&\quad \cdot \frac{1}{\sin\left\{0.5\cos\theta_{mi}\left[\arccos\left(\cos\theta_{mi}-\frac{2.782c}{2\pi f_i dN}\right)-\arccos\left(\cos\theta_{mi}+\frac{2.782c}{2\pi f_i dN}\right)\right]\right\}} \\
&\overset{(a)}{=} \frac{2.782c}{2\pi f_i d\sin\left\{0.5\cos\theta_{mi}\left[\theta_{hi}^{-}-\theta_{hi}^{+}\right]\right\}} \\
&\overset{(b)}{=} \frac{2.782c}{2\pi f_i d\sin\left\{0.5\cos\theta_{mi}\Theta_h(f_i)\right\}} \\
&\overset{(c)}{=} \frac{2.782c}{2\pi f_i d\sin\left(\Theta_{x0}/2\right)},
\end{aligned}
\tag{15}
$$

where (a) is based on the assumption that the two terms in square brackets in the denominator are the half-power direction of the main beam, (b) is based on the definition of the HPBW, and (c) is due to substituting (11). If (10) is substituted into (c) again, we get M, i.e., deriving (15) from the top down and from the bottom up, for the assumption to hold sufficient necessary for the half-power direction $\theta_{hi}^{\pm}$ and satisfies $\theta_{hi}^{-} > \theta_{hi}^{+}$. Therefore, the half-power direction of the frequency squint main beam in elevation can also be noted as

$$
\theta_{hi}^{\pm} = \arccos\left(\cos\theta_{mi} \pm \frac{2.782c}{2\pi f_i dN}\right). \tag{16}
$$

Alternatively, the approximate expression of the above equation can also be obtained by substituting $\beta = kd\cos\theta_m$ into (13) and by a simple derivation, namely

$$
M \approx \frac{2.782c}{2\pi f_i d\sin\left\{\cos\theta_{mi}\arccos\left(\cos\theta_{mi}-\frac{2.782c}{2\pi f_i dN}\right)-\theta_{mi}\cos\theta_{mi}\right\}}. \tag{17}
$$

Since the number of elements on each side of a planar antenna array is an integer, simply rounding to the nearest whole number, we have

$$
\widetilde{M} = \lfloor M \rceil. \tag{18}
$$

First, by investigating the relationship between the main beam direction θ_m and M for the linear array operating at the half-wavelength spacing frequency f_c, we have

$$
M \approx \frac{2.782}{\pi\sin\left\{\cos\theta_m\arccos\left(\cos\theta_m-\frac{2.782}{\pi N}\right)-\theta_m\cos\theta_m\right\}}. \tag{19}
$$

To investigate the relationship between the half-power beam direction and the virtual planar array size, rewrite (19) as

$$
M(f_c,\theta_m) = \frac{2.782}{\pi\sin\left\{0.5\cos\theta_m\left[\arccos\left(\cos\theta_m-\frac{2.782}{\pi N}\right)-\arccos\left(\cos\theta_m+\frac{2.782}{\pi N}\right)\right]\right\}}, \tag{20}
$$

and since from (16) it follows that

$$
\theta_h^{\pm} = \arccos\left(\cos\theta_m \pm \frac{2.782}{\pi N}\right). \tag{21}
$$

Substituting (21) into (20), eventually we get

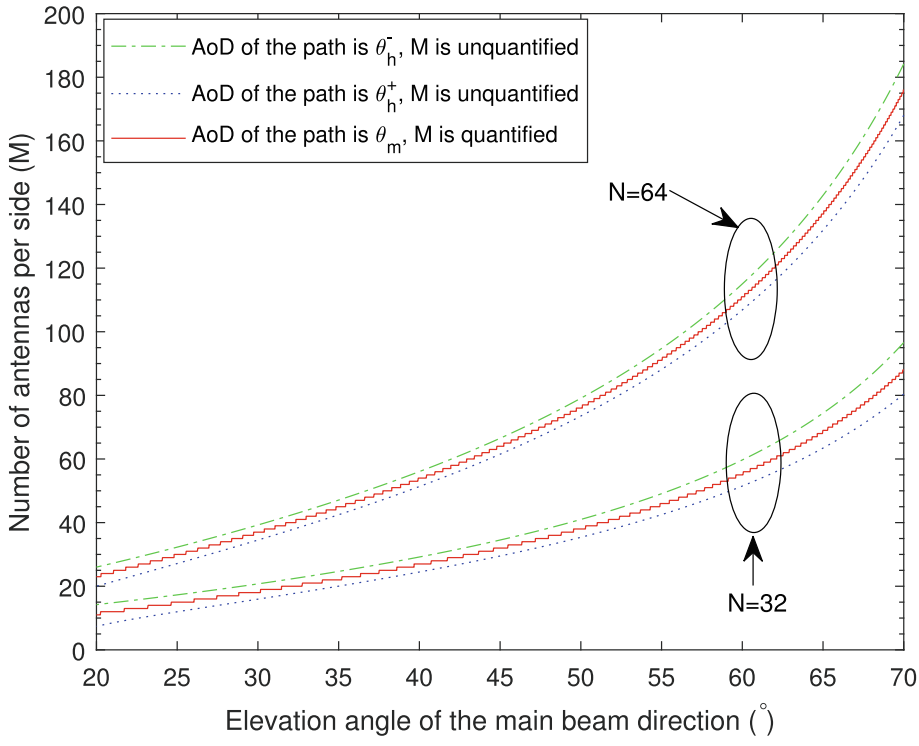

Fig. 2 The main direction of the steering beam of a linear array versus the number of elements per side of a virtual planar antenna array

$$M(f_c,\theta_h^{\pm}) = \frac{\pm 2.782}{\pi \sin\left\{0.5\left(\cos\theta_m \pm \frac{2.782}{\pi N}\right)\left[\theta_m - \arccos\left(\cos\theta_m \pm \frac{2.782}{\pi N}\times 2\right)\right]\right\}}. \quad (22)$$

Note that the half-power direction $\theta_h^{\pm}$ in (22) needs to be kept within $[0°, 90°]$. And since the derivation in (22) is more complicated, there is no analytical comparison for the moment. By simulation experiments, as shown in Fig. 2, in the corresponding main beam angle range satisfying $M(f_c,\theta_h^-) > M(f_c,\theta_h^+)$. Furthermore, since the definition of Θ_{x0} in (c) of (15) is the HPBW of the linear array in the vertical direction, which is independent of the actual beam direction θ_{mi}, it is related to the number of antenna elements. Therefore, it can be assumed that changing the beam direction will cause a change in the number of elements of the virtual planar array. Due to the small angular spread of the mmWave band and the narrow HPBW due to the high number of elements in the array, we use the same virtual planar array to approximate paths in the HPBW range of the same scattering cluster for ease of handling.

Next, we study the relationship between the direction of the frequency squint main beam θ_{mi} and the parameter M of the virtual planar antenna array once the main beam direction θ_m at frequency f_c has been determined. Since a linear array on the z-axis is considered, there is

$$\theta_{mi} = \arccos\left(\frac{c\beta}{2\pi df_i}\right). \quad (23)$$

As the main direction of the beam at frequency f_c is θ_m, substituting into (23) gives $\beta = \pi\cos\theta_m$; again substituting into (23) gives

$$\theta_{mi} = \arccos\left(\frac{c\cos\theta_m}{2df_i}\right). \tag{24}$$

By substituting (24) into (17), we get

$$M(f_i) = \frac{2.782c}{2\pi f_i d} \cdot \frac{1}{\sin\left\{\frac{c\cos\theta_m}{2df_i}\left[\arccos\left(\frac{c}{2df_i}\left(\cos\theta_m - \frac{2.782}{\pi N}\right)\right) - \arccos\left(\frac{c}{2df_i}\cos\theta_m\right)\right]\right\}}. \tag{25}$$

By fixing the array spacing of the virtual planar array to half the wavelength corresponding to the central frequency f_c and rewriting (25), we get

$$M(f_i) = \frac{2.782f_c}{\pi f_i \sin\left\{\frac{f_c\cos\theta_m}{f_i}\left[\arccos\left(\frac{f_c}{f_i}\left(\cos\theta_m - \frac{2.782}{\pi N}\right)\right) - \arccos\left(\frac{f_c}{f_i}\cos\theta_m\right)\right]\right\}}. \tag{26}$$

Figure 3 shows the quantized value M in (26) versus the operating frequency f_i for a central frequency of 45 GHz. In the lower left corner of the curve for the main beam direction $\theta_m = 45°$, there is a part of the frequency with a zero value of M, that is because according to (24), when the squint beam is pointing at $\theta_{mi} = 0°$, its frequency is about 31.92 GHz, and when the frequency is any lower, it is out of the operating frequency range.

According to (55) in Appendix 1, when the maximum angle of the main beam at central frequency f_c is within 60°, i.e., $\theta_m \leq 60°$, if $f_i < \frac{3}{2}f_c$, no grating lobes will appear in the resulting squint beams. When $\theta_m = 60°$, if the operating frequency range is chosen to be $[\frac{1}{2}f_c, \frac{3}{2}f_c)$, the coverage angle range is approximately $\theta_{mi} \in [0°, 70.53°)$.

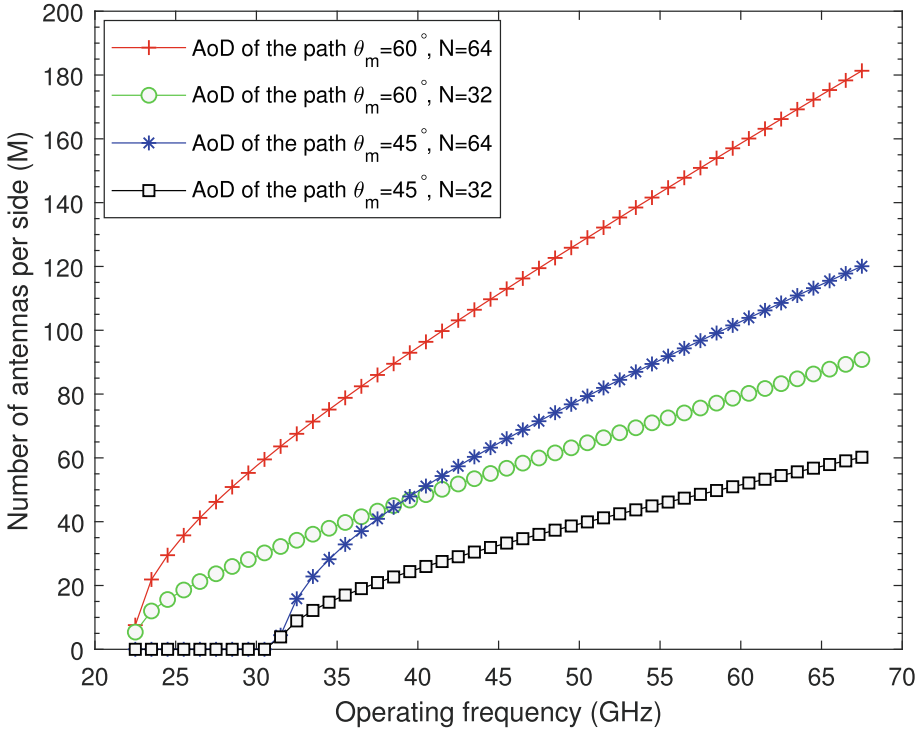

Fig. 3 The number of elements per side of a virtual planar antenna array versus operating frequency

2.2 System model

Following the multi-path scattering Saleh-Valenzuela channel model [5], the channel of a particular user can generally be represented as

$$\mathbf{H} = \sum_{c=1}^{N_c} \sum_{l=1}^{N_{pc}} \alpha_{cl} \mathbf{a}_r \left(\phi_{cl}^r, \theta_{cl}^r\right) \mathbf{a}_t \left(\phi_{cl}^t, \theta_{cl}^t\right)^H, \tag{27}$$

where N_c is the number of all clusters from the BS to that user, N_{pc} is the number of paths within the c^{th} cluster, and $\mathbf{a}_r(\phi_{cl}^r, \theta_{cl}^r)$ and $\mathbf{a}_t(\phi_{cl}^t, \theta_{cl}^t)$ are the steering beam vectors represented by array responses at the receiving and transmitting ends for the l^{th} path in the c^{th} channel cluster, respectively.

For convenience, due to the small angular spread of the beam in the actual mmWave sparse scattering environment, it is assumed that the paths within each cluster can be represented by the array response of the same virtual planar array; if the user has multiple scattering clusters on the same donut-shaped main beam, we still use the array response of the same virtual planar array to approximate the paths in multiple scattering clusters; when the difference in elevation angle between clusters is large, corresponding to several steering donut-shaped beams at the transmitting side, the difference in size of the virtual planar array between clusters is more pronounced, and we assume that the donut-shaped main beam affects a range within the HPBW of the transmitting elevation angle θ_{ring}^t in the real channel environment. According to the approximation of the array factor in (5), the actual channel caused by a particular steering beam of the linear array can then be equivalently expressed as

$$\widetilde{\mathbf{H}}(\theta_{\text{ring}}^t) \approx \sum_{c=1}^{\bar{N}_c} \sum_{l=1}^{\bar{N}_{pc}} \alpha_{cl} \mathbf{a}_r \left(\phi_{cl}^r, \theta_{cl}^r\right) \tilde{\mathbf{a}}_t \left(\phi_{cl}^t, \bar{\theta}_{cl}^t\right)^H, \tag{28}$$

where $\bar{N}_c$ and $\bar{N}_{pc}$ are the number of clusters and paths within the HPBW range of θ_{ring}^t, respectively; the elevation angle $\bar{\theta}_{cl}^t$ in the AoD of each path in the channel needs to be within the HPBW range of θ_{ring}^t at the transmitter side, i.e., satisfying $|\theta_{\text{ring}}^t - \bar{\theta}_{cl}^t| \le \Theta_h\left(f_i\right)/2$, $\bar{\theta}_{cl}^t \in \{\theta_{cl}^t\}$; $\tilde{\mathbf{a}}_t$ is the vector form of the virtual planar array response corresponding to a certain steering beam of the linear array.

When the user at the receiving end uses a square antenna array with M_r elements on each side and placed in the x-y plane, its array response at frequency f_s with the main beam orientated to (ϕ_s^r, θ_s^r) is

$$\begin{aligned}\mathbf{a}_r \left(\phi_s^r, \theta_s^r\right) = & \frac{1}{M_r} \\ & \cdot \Big[1, e^{-j\pi \sin\theta_s^r \cos\phi_s^r f_s/f_c}, \ldots, e^{-j\pi(M_r-1)\sin\theta_s^r \cos\phi_s^r f_s/f_c}, \ldots, \\ & \ldots, e^{-j\pi(M_r-1)\sin\theta_s^r \sin\phi_s^r f_s/f_c}, \ldots, e^{-j\pi(M_r-1)\left(\sin\theta_s^r \cos\phi_s^r + \sin\theta_s^r \sin\phi_s^r\right) f_s/f_c}\Big]^T.\end{aligned} \tag{29}$$

And the array response of the virtual planar array at the transmitter side can be written as

$$\begin{aligned}\tilde{\mathbf{a}}_t \left(\phi_s^t, \theta_s^t\right) = & \frac{1}{\widetilde{M}_t} \\ & \cdot \Big[1, e^{-j\pi \sin\theta_s^t \cos\phi_s^t f_s/f_c}, \ldots, e^{-j\pi(\widetilde{M}_t-1)\sin\theta_s^t \cos\phi_s^t f_s/f_c}, \ldots, \\ & \ldots, e^{-j\pi(\widetilde{M}_t-1)\sin\theta_s^r \sin\phi_s^t f_s/f_c}, \ldots, e^{-j\pi(\widetilde{M}_t-1)\left(\sin\theta_s^t \cos\phi_s^t + \sin\theta_s^t \sin\phi_s^t\right) f_s/f_c}\Big]^T,\end{aligned} \tag{30}$$

where $\widetilde{M}_t$ is the number of elements per side of the virtual array obtained from (18), f_s is the operating frequency, and (ϕ_s^t, θ_s^t) is the virtual main beam direction.

Consequently, the equivalent baseband signal at the user receiver side can be represented as

$$\begin{aligned} y_i =& \sqrt{P}\mathbf{w}_i^H \mathbf{H}_i(f)\,\mathbf{f}\, s_i + \mathbf{w}_i^H n_i(f) \\ \approx& \sqrt{P}\mathbf{a}_r\left(\phi_i^r, \theta_i^r\right)^H \widetilde{\mathbf{H}}\left(\theta_{\text{ring}}^t\right) \sum_{j=1}^{K} \tilde{\mathbf{a}}_t\left(\phi_j^t, \bar{\theta}_{\text{ring}}^t\right) s_i + \mathbf{a}_r\left(\phi_i^r, \theta_i^r\right)^H n_i(f), \end{aligned} \tag{31}$$

where P is the transmitted power of the individual steering beams.

Hence, the rate for this user can be expressed as

$$\begin{aligned} \mathrm{R}_i =& \log_2\left(1 + \frac{P\left|\mathbf{w}_i^H \mathbf{H}_i(f)\mathbf{f}\right|^2}{\sigma_n^2 \mathbf{w}_i^H \mathbf{w}_i}\right) \\ \overset{(d)}{\approx}& \log_2\left(1 + \frac{P|\alpha_l(f)|^2}{\sigma_n^2 \mathbf{w}_i^H \mathbf{w}_i}\left|\mathbf{a}_r\left(\phi_i^r, \theta_i^r\right)^H \mathbf{a}_r\left(\phi_l^r, \theta_l^r\right) \tilde{\mathbf{a}}_t\left(\phi_l^t, \bar{\theta}_l^t\right)^H \tilde{\mathbf{a}}_t\left(\phi_l^t, \theta_{\text{ring}}^t\right)\right|^2\right) \\ \overset{(e)}{\approx}& \log_2\left(1 + \frac{P\left|\alpha_l(f)\tilde{\mathbf{a}}_t\left(\phi_l^t, \bar{\theta}_l^t\right)^H \tilde{\mathbf{a}}_t\left(\phi_l^t, \theta_{\text{ring}}^t\right)\right|^2}{\sigma_n^2}\right), \end{aligned} \tag{32}$$

where (d) is obtained by representing the channel according to (28) as the actual channel generated by a single donut-shaped transmitting main beam in the scattering environment and assuming that the path l with the highest received energy in the actual channel is taken through the steering beam at the receiver end; (e) is assumed that the quantization resolution of the phase shifter of the wideband analog array at the receiver side is high enough to satisfy $\phi_i^r = \phi_l^r$ and $\theta_i^r = \theta_l^r$.

3 User pairing strategies and squint multi-beam algorithms

Figure 4 shows the diagram of a two-user paired NOMA scheme in a downlink multi-user scenario when the BS side is equipped with a linear array and each user end with a planar array, where the linear array is arranged in the z-axis and one of its transmitting steering

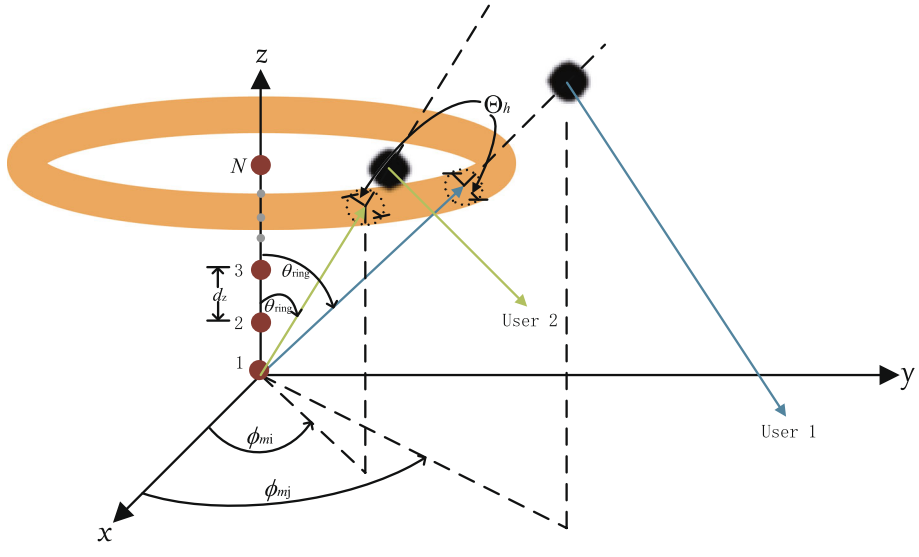

Fig. 4 Downlink NOMA pairing within a donut-shaped main beam at the BS site

beam has two scatterers in its donut-shaped main beam direction, and the corresponding two channel clusters are scattered and directed toward the far user 1 and the near user 2, respectively. The average received energy in the corresponding scattering cluster is smaller for user 1 due to the longer path experienced by the scattering path and the fact that the energy of the longer path is more absorbed in the atmosphere.

Due to the use of the phased linear array at the transmitter side, there is no particularly well-handled solution for inter-user interference on the donut-shaped main beam at the transmitter side [14–16]. On the one hand, we assume that a grouping strategy has been used to serve these users with serious interference using orthogonal resources. On the other hand, it is also possible to pair users with similar departure angles on some of the beams to serve more users through PD-NOMA in the face of unavoidable interference. We classify NOMA pairing strategies into following three categories and discuss their feasibility. Among them, the first strategy is employed in both Algorithms 2 and 3, the second strategy is only used in Algorithm 3, and the last strategy is not included in our algorithms and we have explained its reason. Furthermore, we provide Algorithm 1 for steering the squint beam without any NOMA scheme as a benchmark for comparison.

- NOMA pairing within the direction of a donut-shaped main beam
  This type of NOMA pairing corresponds to Algorithm 2, which selects two users whose channels contain paths with similar departure elevation angles, and the energy difference between these two paths is large enough to consider the PD-NOMA scheme to serve user 2 as well while guaranteeing the minimum required rate for user 1.
- NOMA pairing in the direction of the main beam and its first side lobe
  We attempted to utilize the side lobe direction of a steering beam for pairing to break the distance limit between the two paired users and the BS side in the conventional PD-NOMA scheme. The amplitude of the first side lobe in its dominant direction is −13.465 dB, with a normalized amplitude of about 0.2 (0.212 is more accurate according to equation (6-17) in [6]). It is possible to consider user 2 as the main beam direction user, while there is a scattering path of user 1 in the elevation direction of the donut-shaped first side lobe of the steering beam. In this case, the energy of the corresponding path of user 1 is not necessarily weaker, but since it is the energy of the equivalent channel in the direction of the first side lobe that is significantly weaker than that of user 2, it is also possible to serve simultaneously these two users with significantly different departure elevation angles of the channel path through the PD-NOMA scheme. The corresponding power allocation coefficients β_1 and β_2 are then obtained by applying $0.04|h_1|^2$ to replace the original $|h_1|^2$ as the channel energy for user 1, and the corresponding SIC decoding feasible domain conditions should reformulate (66) and (72) in Appendix 2 as

$$0.04P|h_1|^2 - \left(2^{t_1} - 1\right)\sigma_n^2 > 0, \tag{33}$$

$$\frac{2^{t_1} - 1}{0.04|h_1|^2} + \frac{2^{t_1}\left(2^{t_2} - 1\right)}{|h_2|^2} \leq \frac{P}{\sigma_n^2}. \tag{34}$$

It is found by simulation that the channel coefficients for both user 1 and user 2 are too large in this case, and according to the parameter settings in Fig. 8, approximately

Algorithm 1 Downlink multi-user squint steering beam updation based on a phased linear array at the BS end

Input: The BS obtains the AoD of the PU's new path of the highest energy $\left(\phi_{new}^{t}, \theta_{new}^{t}\right)$ and all SUs' paths of the highest energy $\left\{\left(\phi_{s}^{t}, \theta_{s}^{t}\right)\right\}$; the PU updates its own new arrival angle to $\left(\phi_{new}^{r}, \theta_{new}^{r}\right)$; each SU updates its own arrival angle of the strongest path to $\left(\phi_{s}^{r}, \theta_{s}^{r}\right)$

1: BS $\xleftarrow{f_c} \sum_{k}^{k} \tilde{\mathbf{a}}_t\left(\phi_{k}^{t}, \theta_{new}^{t}\right)$
2: PU $\xleftarrow{f_c} \mathbf{a}_r\left(\phi_{new}^{r}, \theta_{new}^{r}\right)$
3: **for all** SUs **do**
4: Update $\left(\phi_{s}^{t}, \theta_{s}^{t}\right)$ and $\left(\phi_{s}^{r}, \theta_{s}^{r}\right)$ for this SU
5: **if** $\theta_{s}^{t} \in \left[\theta_{new}^{t} - i\Theta_h/2, \theta_{new}^{t} + i\Theta_h/2\right]$ and $IsGroupActivated(G_i) == false$ **then**
6: $f_s = f_c \cos\theta_{new}^{t} / \cos\theta_{s}^{t}$
7: BS $\xleftarrow{f_s} \sum_{k}^{k} \tilde{\mathbf{a}}_t\left(\phi_{k}^{t}, \theta_{new}^{t}\right)$, feeds back f_s to SU, and marks $IsGroupActivated(G_i) = true$ and $IsUserServed(\mathrm{SU}) = true$
8: SU $\xleftarrow{f_s} \mathbf{a}_r\left(\phi_{s}^{r}, \theta_{s}^{r}\right)$
9: **end if**
10: **end for**
11: **for all** SUs with $IsUserServed(\mathrm{SU}) == false$ **do**
12: The BS rejects the enhanced beam service for this SU, reports and feeds back the request result
13: **end for**

$|h_1|^2 > 4$ needs to be satisfied. This magnitude requirement is too large for a single-antenna scenario. For scenarios using array antennas, there is some feasibility due to the array gain at the transceiver end, which will be demonstrated in Algorithm 3 and verified by simulation experiments.

- NOMA pairing in the direction of the main beam and its grating lobe
  Pairing between the main beam and grating lobe directions is also possible; however, the presence of a grating lobe would reduce the transmit power in the main beam direction while maintaining a uniform transmit power for each beam. This pairing is not adopted for the time being, since in this paper the squint beam is applied and there is no need to provide multi-beam with grating lobes. It is possible to circumvent this by limiting the maximum elevation angle of the main beam and the maximum working frequency of the squint beam, according to the conditions given in the forepart of Appendix 1 for a wideband array not to create a grating lobe.

3.1 Benchmark: downlink frequency squint multi-beam algorithm without PD-NOMA

Algorithm 1 draws on the idea of grouping in [8] and does not use the scheme of the PD-NOMA. For convenience, the user operating at the central frequency f_c is referred to as the primary user (PU) and the users operating at other frequencies are referred to as secondary users (SUs).

In step 1, the BS updates the array response of its steering beam at frequency f_c according to the elevation angle $\theta_{\mathrm{new}}^{t}$ in the AoD of the strongest path of the PU. According to

(30) and (31), the steering beam of the linear array is approximated by the steering beams of a virtual planar array.

In step 2, the PU calculates the receiving array response from (29) based on the new arrival angle $(\theta^r_{\text{new}}, \phi^r_{\text{new}})$ and operating at frequency f_c to generate the received beam.

In step 5, the elevation angle space at the transmitter end is divided into angular regions by the HPBW Θ_h at the central frequency of the PU, with each region supporting at most one donut-shaped squint main beam within the angular range, and each steering beam serving at most one user at a time. It is obtained from (6) and (7) resulting in

$$\Theta_h\left(f_c\right) \approx \left|\arccos\left(\cos\theta_m - \frac{2.782}{\pi N}\right) - \arccos\left(\cos\theta_m + \frac{2.782}{\pi N}\right)\right|. \tag{35}$$

IsGroupActivated$(\cdot)$ indicates whether a particular transmit elevation interval group is occupied by *true* or *false*, and the default value is *false*.

In step 6, since the BS side uses a wideband phased array and the phase shifters therein are unquantized ideal ones, the operating frequency of the desired squint beam f_s can be calculated from (54).

In step 7, the BS reuses the PU's array response at frequency f_s, marks this transmit elevation interval group as occupied, and feeds back f_s to that user. *IsUserServed*$(\cdot)$ indicates whether a particular SU is served by *true* or *false*, and the default value is *false*.

In step 8, the SU calculates the array response based on the new arriving angle (θ^r_s, ϕ^r_s) and f_s from (29) and works at frequency f_s to produce the reception beam.

3.2 The enhanced beam squint algorithm supporting PD-NOMA in the donut-shaped main beam

Algorithm 2 improves on Algorithm 1 by enabling each donut-shaped squint main beam at the transmitting side to serve two users simultaneously via the PD-NOMA.

The work in [17] gives the achievable rate of NOMA users when a single antenna is employed at both the transmitter and receiver, while in this paper, since the BS uses a linear array and each user uses a planar array, the achievable rate of users in the two-user NOMA pairing scheme can be written as

$$R_2 = \log_2\left(1 + \frac{\beta_2 P\left|\mathbf{a}_r\left(\phi^r_{s2}, \theta^r_{s2}\right)^H \widetilde{\mathbf{H}}_2 \widetilde{\mathbf{a}}_t\left(\phi^t_{s2}, \theta^t_s\right)\right|^2}{\sigma_n^2}\right), \tag{36}$$

$$R_1 = \log_2\left(1 + \frac{\beta_1 P\left|\mathbf{a}_r\left(\phi^r_{s1}, \theta^r_{s1}\right)^H \widetilde{\mathbf{H}}_1 \widetilde{\mathbf{a}}_t\left(\phi^t_{s1}, \theta^t_s\right)\right|^2}{\beta_2 P\left|\mathbf{a}_r\left(\phi^r_{s1}, \theta^r_{s1}\right)^H \widetilde{\mathbf{H}}_1 \widetilde{\mathbf{a}}_t\left(\phi^t_{s1}, \theta^t_s\right)\right|^2 + \sigma_n^2}\right). \tag{37}$$

By replacing the values $|h_1|^2$ and $|h_2|^2$ for the single-antenna baseband signal in (63) and (64) in Appendix 2 with the corresponding values under the equivalent baseband signal of the antenna array, respectively $\left|\mathbf{a}_r\left(\phi^r_{s1}, \theta^r_{s1}\right)^H \widetilde{\mathbf{H}}_1 \widetilde{\mathbf{a}}_t\left(\phi^t_{s1}, \theta^t_s\right)\right|^2$ and $\left|\mathbf{a}_r\left(\phi^r_{s2}, \theta^r_{s2}\right)^H \widetilde{\mathbf{H}}_2 \widetilde{\mathbf{a}}_t\left(\phi^t_{s2}, \theta^t_s\right)\right|^2$, we get

Algorithm 2 Enhanced downlink squint beam updation with PD-NOMA pairing in the main direction of each steering beam

Input: The BS obtains the AoD of the primary user's new path of the highest energy $\left(\theta_{new}^{t}, \phi_{new}^{t}\right)$ and all SUs' paths of the highest energy $\left\{\left(\theta_{s}^{t}, \phi_{s}^{t}\right)\right\}$; the PU updates its own new arrival angle to $\left(\theta_{new}^{r}, \phi_{new}^{r}\right)$; each SU updates its own arrival angle of the strongest path to $\left(\theta_{s}^{r}, \phi_{s}^{r}\right)$

1: The BS divides the departure elevation angle into groups according to $\theta_{s}^{t} \in \left[\theta_{new}^{t} - i\Theta_{h}/2, \theta_{new}^{t} + i\Theta_{h}/2\right]$ and selects user 2 and user 1's optional set for each group G_i
2: BS $\xleftarrow{f_c} \sum^{k} \tilde{\mathbf{a}}_t\left(\phi_{k}^{t}, \theta_{new}^{t}\right)$
3: PU $\xleftarrow{f_c} \mathbf{a}_r\left(\phi_{new}^{r}, \theta_{new}^{r}\right)$
4: **for all** G_i with $i \neq 0$ **do**
5: **for all** user 1 in user 1's optional set **do**
6: $f_s = f_c \cos\theta_{new}^{t} / \cos\left[\left(\theta_{s1}^{t} + \theta_{s2}^{t}\right)/2\right]$
7: The BS calculates β_1 and β_2
8: **if** $\beta_2 \leq \beta_2^{max}$ **then**
9: BS $\xleftarrow{f_s}$ $\sum^{k} \tilde{\mathbf{a}}_t\left(\phi_{k}^{t}, \theta_{new}^{t}\right)$, feeds back f_s to users 1 and 2, marks *IsGroupActivated*(G_i) = *true*, *IsUserPaired*(user 1) = *true*, *IsUserPaired*(user 2) = *true*, *IsUserServed*(user 1) = *true*, *IsUserServed*(user 2) = *true*
10: user 1 $\xleftarrow{f_s} \mathbf{a}_r\left(\phi_{s1}^{r}, \theta_{s1}^{r}\right)$, user 2 $\xleftarrow{f_s} \mathbf{a}_r\left(\phi_{s2}^{r}, \theta_{s2}^{r}\right)$, and **break**
11: **end if**
12: **end for**
13: **if** *IsGroupActivated*$(G_i) ==$ *false* and user 2 $\neq$ *null* **then**
14: Executes Steps 6-8 in Algorithm 1 for user 2
15: **end if**
16: **end for**
17: **for all** SUs with *IsUserServed*(SU) $==$ *false* **do**
18: The BS rejects the enhanced beam service for this SU, reports and feeds back the request result
19: **end for**

$$\beta_1 = \frac{\left(2^{t_1} - 1\right)\left(P\left|\mathbf{a}_r\left(\phi_{s1}^{r}, \theta_{s1}^{r}\right)^{H}\widetilde{\mathbf{H}}_1\widetilde{\mathbf{a}}_t\left(\phi_{s1}^{t}, \theta_{s}^{t}\right)\right|^2 + \sigma_n^2\right)}{2^{t_1}P\left|\mathbf{a}_r\left(\phi_{s1}^{r}, \theta_{s1}^{r}\right)^{H}\widetilde{\mathbf{H}}_1\widetilde{\mathbf{a}}_t\left(\phi_{s1}^{t}, \theta_{s}^{t}\right)\right|^2}, \tag{38}$$

$$\beta_2 = \frac{P\left|\mathbf{a}_r\left(\phi_{s1}^{r}, \theta_{s1}^{r}\right)^{H}\widetilde{\mathbf{H}}_1\widetilde{\mathbf{a}}_t\left(\phi_{s1}^{t}, \theta_{s}^{t}\right)\right|^2 - \left(2^{t_1} - 1\right)\sigma_n^2}{2^{t_1}P\left|\mathbf{a}_r\left(\phi_{s1}^{r}, \theta_{s1}^{r}\right)^{H}\widetilde{\mathbf{H}}_1\widetilde{\mathbf{a}}_t\left(\phi_{s1}^{t}, \theta_{s}^{t}\right)\right|^2}. \tag{39}$$

Note that NOMA pairing requires that user 2 be able to decode user 1's signal through the SIC, so the maximum transmit power coefficient of user 2 is limited to $\beta_2^{\max}$ in step 1, and after selecting user 2, user 1 is chosen exhaustively until a suitable size of β_2 is picked.

In step 1, the BS divides the departure elevation angle into intervals according to $\theta_{s}^{t} \in \left[\theta_{\text{new}}^{t} - i\Theta_{h}/2, \theta_{\text{new}}^{t} + i\Theta_{h}/2\right]$, and in each interval, if there is a user path, then choose

the one with the strongest channel energy as user 2 in the NOMA pair; if there are other users, then treat them as users in the feasible set of user 1 in this group.

Note that since the interval is divided only by the HPBW of the elevation angle corresponding to the frequency f_c, it is possible that when $f_s > f_c$ could result in the departure angle of the strongest path of the selected paired user being outside the HPBW range where the actual squint main beam is located, thus reducing the rate performance of the user in the interval. This problem is potentially inherent in both Algorithms 2 and 3, and a more reasonable way of grouping by angular space division is subject to further investigation. However, it is ignored for the moment in this paper as it is more concerned with increasing the number of simultaneous users served through PD-NOMA groups.

In step 4, the selection of the group G_i with $i \neq 0$ is due to the assumption that the PD-NOMA scheme is used only in squint beams.

In step 5, the departure angles of the strongest paths of users 1 and 2 in the NOMA pair are denoted as $\left(\theta_{s1}^t, \phi_{s1}^t\right)$ and $\left(\theta_{s2}^t, \phi_{s2}^t\right)$, respectively, and the arrival angles of the corresponding paths of the two users are denoted as $\left(\theta_{s1}^r, \phi_{s1}^r\right)$ and $\left(\theta_{s2}^r, \phi_{s2}^r\right)$, respectively.

In step 6, the BS takes $\left(\theta_{s1}^t + \theta_{s2}^t\right)/2$ as the transmit elevation angle θ_s^t of the steering beam in this interval and calculates its operating frequency from $f_s = f_c \cos\theta_{\text{new}}^t / \cos\theta_s^t$.

In step 7, the BS allocates transmitted power coefficients β_1 and β_2 within the beam to the users in this NOMA pair according to (38) and (39).

In step 9, the BS reuses the array response of the PU at frequency f_s and feedback f_s to the users within this NOMA pair. *IsUserPaired*$(\cdot)$ indicates whether a particular SU is served in a NOMA group by *true* or *false*, and the default value is *false*.

In step 10, users 1 and 2 within the NOMA pair calculate the array response based on the new arrival angles $\left(\theta_{s1}^r, \phi_{s1}^r\right)$ and $\left(\theta_{s2}^r, \phi_{s2}^r\right)$ as well as the new squint frequency f_s from (29) and work on the frequency f_s to generate the receiving beam, respectively. After that, it jumps out of the inner loop at the BS side.

3.3 The enhanced beam squint algorithm supporting NOMA pairing of the main beam direction with the first side lobe direction

Algorithm 3 improves on Algorithm 2 by supporting the PD-NOMA opportunity communication for pairing between a user in the direction of the squint main beam and a user in the direction of its first side lobe. The general idea is to select a group with only one active user and find a suitable unserved user in the first side lobe direction of the steering beam in the group for pairing as NOMA user 1.

To avoid the concept of defining the HPBW in the direction of the first side lobe, we assume that the direction of the first side lobe points exactly to the strongest path of NOMA user 1. By exhaustively enumerating the unserved users as NOMA user 1, the operating frequency f_i and the main direction θ_{mi} of the squint beam corresponding to the direction of its strongest path can be obtained from the direction θ_{s1} of NOMA user 1, assuming that NOMA user 1 has been selected and from equation (6-16a) in [6], the first side lobe direction of this steering beam is given by

$$\theta_{s1}\left(f_i\right) = \arccos\left(\cos\theta_{mi} \pm \frac{3f_c}{Nf_i}\right). \tag{40}$$

Algorithm 3 Enhanced squint beam updation supporting PD-NOMA between the main beam direction and the first side lobe direction for each steering beam

Input: When Algorithm 2 jumps out of its Step 16

1: **for all** SUs with *IsUserServed*(SU) == *false* **do**
2: Treats this SU as user 1 in the first side lobe NOMA pair and sets $\theta_{s1}^{+} = \theta_{s1}^{t}$, calculates $f_i = \left(\cos\theta_m + \frac{3}{N}\right) f_c / \cos\theta_{s1}^{+}$ and $\theta_{hi}^{\pm} = \arccos\left[\left(\cos\theta_m \pm \frac{2.782}{\pi N}\right)\frac{c}{2df_i}\right]$
3: **for all** SUs with *IsUserServed*(SU) == *true* and *IsUserPaired*(SU) == *false* **do**
4: **if** $\theta_s^t \in \left[\theta_{hi}^{+}, \theta_{hi}^{-}\right]$ **then**
5: Treats this SU as user 2 in the first side lobe NOMA pair and calculates β_1 and β_2
6: **if** $\beta_2 \le \beta_2^{max}$ **then**
7: BS $\xleftarrow{f_i} \sum_{k}^{k} \tilde{\mathbf{a}}_t\left(\phi_k^t, \theta_{new}^t\right)$, feeds back f_i to users 1 and 2 in the NOMA pair
8: user 1 $\xleftarrow{f_i} \mathbf{a}_r\left(\phi_{s1}^r, \theta_{s1}^r\right)$, user 2 $\xleftarrow{f_i} \mathbf{a}_r\left(\phi_{s2}^r, \theta_{s2}^r\right)$
9: Marks *IsUserPaired*(user 1) = *true*, *IsUserPaired*(user 2) = *true*, *IsUserServed*(user 1) = *true*, and **break**
10: **end if**
11: **end if**
12: **end for**
13: **end for**
14: **for all** SUs with *IsUserServed*(SU) == *false* **do**
15: The BS rejects the enhanced beam service for this SU, reports and feeds back the request result
16: **end for**

Substituting (54) into (40) gives the relationship between the direction of the first side lobe and the operating frequency, as

$$f_i = \left(\cos\theta_m \pm \frac{3}{N}\right) f_c / \cos\theta_{s1}^{\pm}. \tag{41}$$

In step 2, the elevation angle in the AoD of this SU's strongest path as the first side lobe direction $\theta_{s1}^{\pm}$, the corresponding squint frequency f_i of the new squint main beam is obtained from (41). To guarantee the validity of the HPBW range and power distribution coefficients in the simulation, set $f_i = \left(\cos\theta_m + \frac{3}{N}\right) f_c / \cos\theta_{s1}^{+}$.

After the operating frequency f_i has been determined, the half-power beam angle range $\left[\theta_{hi}^{+}, \theta_{hi}^{-}\right]$ for the main direction of this squint beam can be obtained, and within this angle range, the user who occupies a steering beam alone is matched as user 2 in the NOMA pair, and then the array response of the PU's transmitted beam is multiplexed at frequency f_i to serve this NOMA pair, where there is

$$\theta_{m\_User2}^{t} \in \left[\theta_{hi}^{+}, \theta_{hi}^{-}\right]. \tag{42}$$

According to (21) the half-power direction of this main beam is

$$\theta_{hi}^{\pm} = \arccos\left(\cos\theta_{mi} \pm \frac{2.782 f_c}{\pi N f_i}\right), \tag{43}$$

alternatively it can be written as

$$\theta_{hi}^{\pm} = \arccos\left[\left(\cos\theta_m \pm \frac{2.782}{\pi N}\right)\frac{f_c}{f_i}\right]. \tag{44}$$

In step 5, treat the selected SU as user 2 in the first side lobe NOMA pair and calculate the power allocation coefficients β_1 and β_2 from (45) and (46). When calculating the power allocation coefficients, the equivalent channel energy of user 1 should be multiplied by 0.04, since it is in the direction of the first side lobe of the transmitting beam. Therefore, the power allocation coefficients in the NOMA pair should vary from (38) and (39) to

$$\beta_1 = \frac{\left(2^{t_1}-1\right)\left(0.04P\left|\mathbf{a}_r\left(\phi_{s1}^r,\theta_{s1}^r\right)^H\widetilde{\mathbf{H}}_1\widetilde{\mathbf{a}}_t\left(\phi_{s1}^t,\theta_s^t\right)\right|^2+\sigma_n^2\right)}{2^{t_1}\times 0.04P\left|\mathbf{a}_r\left(\phi_{s1}^r,\theta_{s1}^r\right)^H\widetilde{\mathbf{H}}_1\widetilde{\mathbf{a}}_t\left(\phi_{s1}^t,\theta_s^t\right)\right|^2}, \tag{45}$$

$$\beta_2 = \frac{0.04P\left|\mathbf{a}_r\left(\phi_{s1}^r,\theta_{s1}^r\right)^H\widetilde{\mathbf{H}}_1\widetilde{\mathbf{a}}_t\left(\phi_{s1}^t,\theta_s^t\right)\right|^2-\left(2^{t_1}-1\right)\sigma_n^2}{2^{t_1}\times 0.04P\left|\mathbf{a}_r\left(\phi_{s1}^r,\theta_{s1}^r\right)^H\widetilde{\mathbf{H}}_1\widetilde{\mathbf{a}}_t\left(\phi_{s1}^t,\theta_s^t\right)\right|^2}. \tag{46}$$

Since the user in the first side lobe direction is selected as user 1 in the NOMA pair before selecting user 2 in Algorithm 3, there is no need to adjust the frequency of the squint beam in the process of selecting NOMA user 2, thus avoiding the situation where the operating frequency determined by user 1 in the NOMA pair causes the strongest path of user 2 to be outside the HBPW of the squint main beam, resulting from the selection of NOMA user 2 first.

In step 8, users 1 and 2 within the NOMA pair calculate the array response based on the new arrival angles $\left(\theta_{s1}^r,\phi_{s1}^r\right)$ and $\left(\theta_{s2}^r,\phi_{s2}^r\right)$ as well as the new squint frequency f_i from (29) and work on the frequency f_i to generate the receiving beam, respectively.

In step 9, the BS marks users 1 and 2 as users in a NOMA pair and jumps out of the inner loop.

4 Results and discussion

The simulations in this section are based on a uni-cell scenario with one BS and multi-user, where the BS side consists of a linear array of N_t antenna elements, the total number of users is N_u and each user end uses a square planar array with M_r elements on each side, and all transceivers are wideband phased antenna arrays with central frequency f_c of 45 GHz and element spacing of $\lambda_c/2$. It is assumed that the linear array of the transmitting BS is placed in the z-axis, while the planar array of the receiving end is placed in the x-y plane of the user's respective coordinate system and that both the elevation angle θ_{mi} and the azimuth angle $\phi_m(f_i)$ of the main beam at both the transceiver ends are within $[0°, 90°]$. The elevation angle θ_m of a PU transmitted beam is limited to $[30°, 60°]$ for more efficient use of the squint beam, and the operating frequency interval of the squint beam is limited to $[f_c/2, 3f_c/2]$ for avoiding the appearance of grating lobes and an excessive number of elements in the virtual planar array.

Similar to [3], we use the extended Saleh-Valenzuela channel model [4] for the mmWave band to model the user's channel, with each user operating at its own frequency and its channel consisting of several clusters with a number of paths in each cluster, each of which is described by multiplying the product of the array response of the transmitting and receiving steering beams by the channel coefficient. Specifically, the difference in the scattering environment between users is represented by the number of clusters per user

channel which is randomly chosen between 1 and 8, and the number of paths per cluster which is randomly picked between 1 and 10. The mean cluster angle of the scattering clusters of each user follows a uniform distribution, and the arrival and departure angles of the paths within the clusters each follows a Laplacian distribution with a standard deviation of this cluster angle spread, which is held for all clusters at 7.5°. The signal and noise both independently obey a Gaussian distribution with mean 0 and standard deviation of 1, i.e., $\mathcal{CN}(0,1)$, and assume that the scenario is noise limited such that $\frac{P}{\sigma_n^2} = 1$. Note that the maximum number of steering beams at the BS side is constrained by its power constraint in practice, which is not limited in the simulation; the channel of the i^{th} cluster of a user satisfies $\mathbb{E}\left[\|\mathbf{H_i}\|_F^2\right] = N_t N_r$, where N_t is the actual number of antennas in the transmitting linear array, $N_r = M_r^2$, α_{il} is the complex gain coefficient of the l^{th} path within its i^{th} cluster, and its value obeys the i.i.d. complex Gaussian distribution $\mathcal{CN}\left(0, \sigma_{\alpha,i}^2\right)$, where $\sigma_{\alpha,i}^2 = \frac{N_t N_r}{N_{pi}}$ is the average power of the internal path of this cluster. And to simplify the design, only the direction of the maximum energy path of each user is actually selected by the transceiver for the direction of the steering beam, which avoids the problem of dimension mismatch of the transmit steering beam between multi-cluster caused by inconsistent virtual planar array sizes by assuming that only one cluster in the channel needs to be handled. Finally, all results are reported for averaged over 5000 random channel realizations. Unless otherwise mentioned, these parameters are used for the experiments.

Figure 5 compares the number of simultaneous users served when the BS is equipped with a linear array and a planar array, respectively, using benchmark Algorithm 1. For

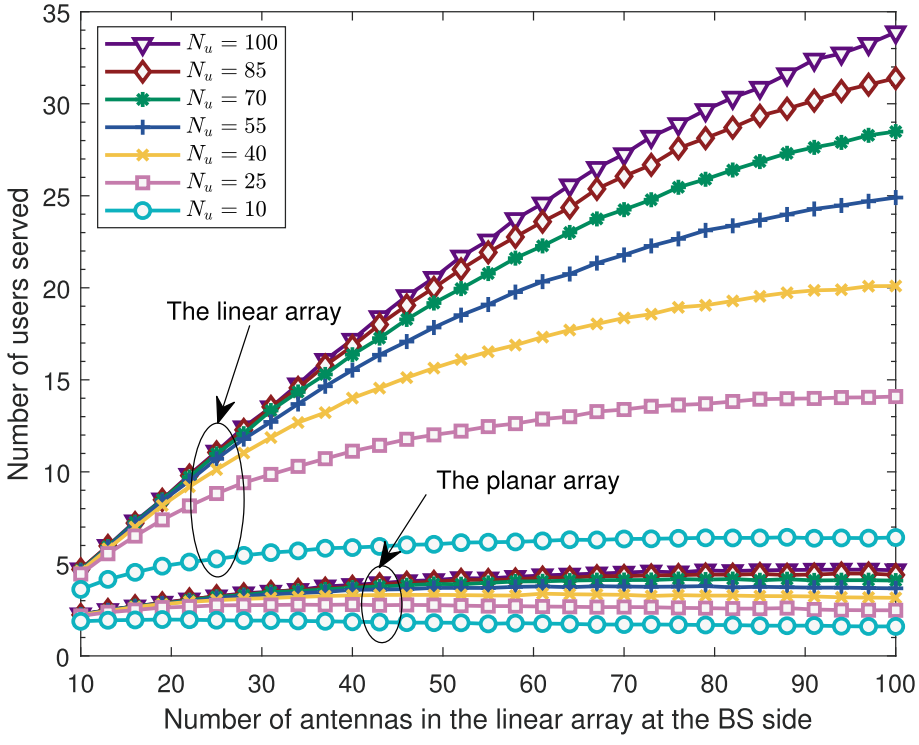

Fig. 5 Comparison of the number of simultaneous users served by benchmark Algorithm 1 when the BS side is equipped with a linear array and a planar array, respectively

fairness, when the number of antennas of the linear array is determined, the number of antennas of the planar array is selected in such a way that the steering beams of both are pointed at the same path and the HPBWs in the vertical direction of the two squint main beams are basically the same. The number of users served of the linear array is significantly better than that of the planar array due to the constraint of the horizontal main direction of the squint steering beam of the planar array, and the more users in the system, the more significant it is.

Figures 6 and 7 compare the number of simultaneous users served and the sum rate performance of the system for the three proposed algorithms in two scenarios with the number of linear array antennas at the BS side of 32 and 64 while keeping $N_r = 64$ for all users and with t_1 taken at 2 bits/s/Hz. As the transmit elevation angle is divided into groups by the HPBW of the steering beam of the array at the BS side, the HPBW is larger when the number of antennas is smaller, and the angle interval per group is larger and the number of groups divided is smaller. Specifically, the number of groups varies depending on the direction of the main user's transmit beam, with about 15 intervals at $N_t = 32$ and more than 40 intervals at $N_t = 64$. Therefore, when the number of antennas at the BS side is smaller, it is easier to have serviceable users within a group for the same number of users in the system. Consequently, with the limitation on the number of users that can be served simultaneously in each group, it is easier to reach saturation with active users in each group as the number of users to be served in the system increases.

The sum rate performance of the three proposed algorithms is compared in Fig. 6. It can be seen that the sum rates of all three algorithms are significantly higher in the configuration for $N_t = 64$ than for $N_t = 32$; the sum rates of Algorithm 1 are higher than those of Algorithms 2 and 3 in each configuration, while the sum rates of Algorithm 2 are slightly higher than those of Algorithm 3, which are closer to each other. When the number of antennas at the BS side is $N_t = 32$, the increasing trend of the sum rate in the system smoothes out significantly as the number of users in the system increases, which is due to the fact that each group is basically served by users as the number of users increases. For $N_t = 64$, there is only a moderating trend in the sum rate as the number of users increases. This is due to the fact that more antennas at the transmitter end divide more intervals, and the number of users in the graph is not yet such that there is a greater probability that each interval will have a serving user.

The performance of the proposed three algorithms in terms of the number of simultaneous users served is compared in Fig. 7. For the total number of users to be served simultaneously in the system, the performance of all three algorithms in the $N_t = 64$ configuration is higher than when $N_t = 32$; as the number of users to be served in the system increases, the curves of the three algorithms in the $N_t = 32$ configuration flatten out significantly; thanks to the larger number of groups and that each group can serve more users at the same time through the PD-NOMA, at $N_t = 64$, the moderating trend of the boost in the curves of the number of users served simultaneously by Algorithms 2 and 3 is not as pronounced as in Algorithm 1. In addition, there is an intersection point in the curves of the number of NOMA served simultaneously in the system for both antenna configurations. At the beginning, when the number of users to be served in the system is low, the number of NOMA users served is smaller for $N_t = 64$ than for $N_t = 32$. This is due to the fact that with more antennas at the transmitter there are more grouping intervals and the users served are more likely to be in separate groups and therefore

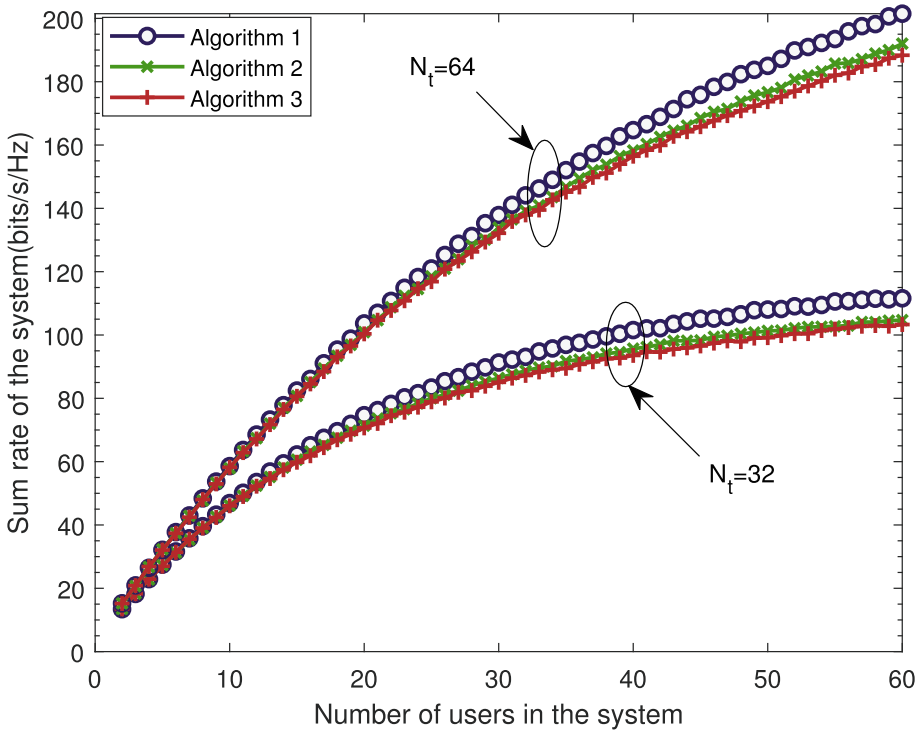

Fig. 6 Comparison of sum rates in the system when using the proposed algorithms

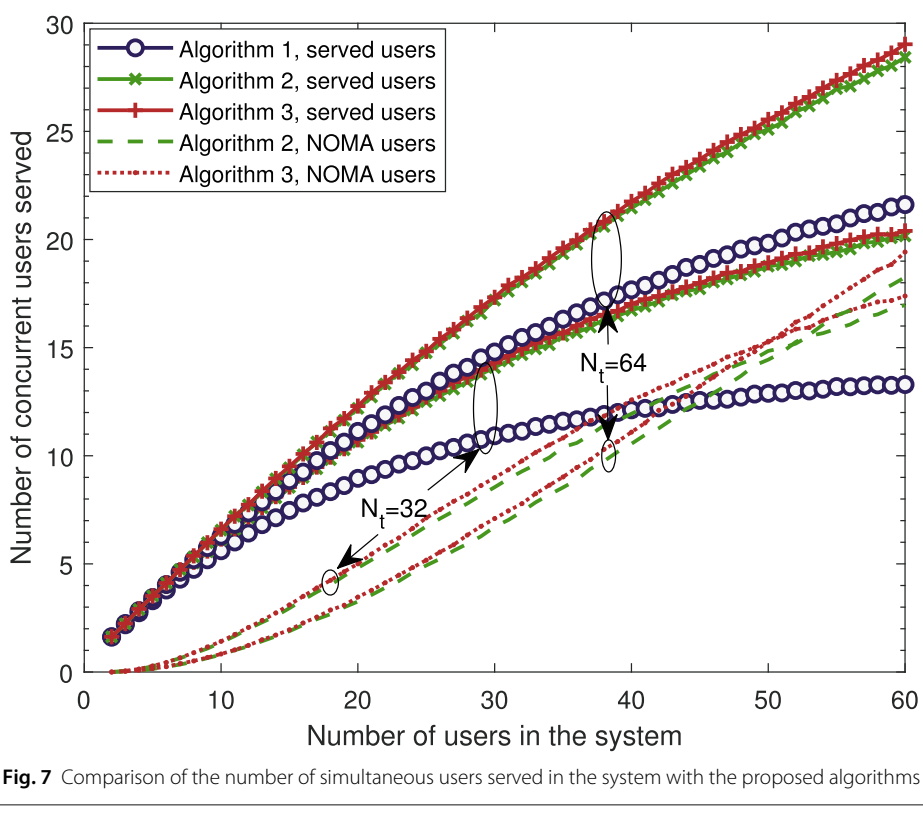

Fig. 7 Comparison of the number of simultaneous users served in the system with the proposed algorithms

have less opportunity for NOMA pairing. As the number of NOMA users served rises, starting at about 15 users in the figure, the number of NOMA users in the two algorithms for $N_t = 32$ is smaller than for $N_t = 64$, due to the larger range of angles per grouping interval at $N_t = 32$, and as the number of active grouping pairs in the system becomes larger, additional users to be served with the strongest path of elevation angles in the AoD have a significantly higher probability of appearing in the paired groupings. In contrast, with $N_t = 64$, there is still a higher probability that a newly added user to be served will appear in an unpaired grouping when there are the same number of grouping pairs in the system because of the greater number of group intervals divided.

Comparing Figs. 6 and 7, compared to Algorithm 1, Algorithms 2 and 3 increase the number of simultaneous served users but decrease the sum rate in the system, due to the fact that when NOMA pairing is successful, part of the transmit power is allocated to NOMA user 1, which has a poor channel condition, reducing the rate of NOMA user 2, which has a better channel condition. Compared to Algorithm 2, Algorithm 3 slightly increases the number of NOMA users served simultaneously in the system; however, it also further reduces the sum rate of the system due to the increased power allocated to NOMA user 1 in the side lobe NOMA pair. Since the number of simultaneous NOMA users served simultaneously in Algorithms 2 and 3 is similar for the same antenna configuration, it can be seen that the number of successful side lobe NOMA pairs in Algorithm 3 is extremely small, and as Algorithm 3 is more complex than Algorithm 2, it is generally better to employ only Algorithm 2 to increase the number of simultaneous users served in the system.

5 Conclusion

In this article, we studied the downlink cellular communication scheme for serving multi-user through a wideband phased linear array at the BS side with frequency squint beams. First, a method using steering main beams of a virtual planar array to simulate the donut-shaped main beam of the linear array was proposed to solve the matching problem of the steering main beam and the channel model. Then, an algorithm drawing on the concept of JSDM grouping to divide the transmitter elevation angle interval into multiple small intervals and serve multi-user by means of squint beams from the linear array was proposed, where at most one user can be served by a single squint beam in each small interval. Subsequently, the algorithm supporting PD-NOMA for two users whose transmit channel path directions are both within the half-power beam range of a single quint donut-shaped main beam and the algorithm which supports PD-NOMA pairing of the main direction of a single squint beam and its first side lobe direction were raised for serving more users, for which the feasible domain of a two-user PD-NOMA channel for a given SIC decoding power constraint in the single-antenna scenario was briefly discussed and placed in Appendix 2 for consistency and conciseness in the bulk of the paper. The feasibility of the proposed scheme and the performance of the proposed algorithms were finally verified by simulation.

Appendix 1. The condition for only one grating lobe occurring in a steering beam of the wideband linear array

In (2), let $\psi = 0$, we can get the main beam direction of each frequency as

$$\cos\theta_{mi} = \frac{c\beta}{2\pi f_i d}. \tag{47}$$

We start by deriving the necessary conditions for not generating a grating lobe in the steering beam. Since the presence of a grating lobe requires $|\psi| = 2m\pi, \quad m = 1, 2, \cdots$, the condition that $|\psi| < 2\pi$ must be satisfied if a grating lobe is to be avoided, namely

$$|kd\cos\theta - \beta| < 2\pi. \tag{48}$$

Substituting $\beta = kd\cos\theta_{mi}$ into (48), we have

$$kd|\cos\theta - \cos\theta_{mi}| < 2\pi. \tag{49}$$

Replacing $k = 2\pi f_i/c$ in (2) and expanding the absolute value of the left term in the inequality, we get

$$\cos\theta_{mi} - \frac{2f_c}{f_i} < \cos\theta < \cos\theta_{mi} + \frac{2f_c}{f_i}. \tag{50}$$

Since $|\cos\theta| \le 1$, for (50) to hold constant, requires satisfying

$$\cos\theta_{mi} + \frac{2f_c}{f_i} > 1, \tag{51a}$$

$$\cos\theta_{mi} - \frac{2f_c}{f_i} < -1. \tag{51b}$$

Namely, we have

$$f_i < \frac{2f_c}{1 - \cos\theta_{mi}}, \tag{52a}$$

$$f_i < \frac{2f_c}{1 + \cos\theta_{mi}}. \tag{52b}$$

Since the main beam direction is kept only in the interval $[0, \frac{\pi}{2})$, thus $\cos\theta_{mi} > 0$, it follows that $\frac{2f_c}{1+\cos\theta_{mi}} < \frac{2f_c}{1-\cos\theta_{mi}}$. For readability, rewrite (24) as

$$\theta_{mi} = \arccos\left(\frac{f_c}{f_i}\cos\theta_m\right), \tag{53}$$

which equals

$$\cos\theta_{mi} f_i = \cos\theta_m f_c. \tag{54}$$

It shows the relationship between the working frequency of the squint beam and the main directional elevation angle. Thanks to the ideal phase shifters used in the wideband phased array, making β independent of frequency, whose value $\beta = \pi\cos\theta_{mi} f_i/f_c$ can be calculated from the beam direction at a particular frequency, such as the beam direction of $\cos\theta_m$ when operating at f_c, which also reveals the physical meaning implicit in (54).

Substituting (53) into (52b) gives

$$f_i < (2 - \cos\theta_m) f_c. \tag{55}$$

On the other hand, by the positive value of β in (48), as the antenna spacing increases, if there is only one grating lobe, then $\psi = -2\pi$. If no grating lobe should emerge, it needs to satisfy

$$kd\cos\theta - \beta > -2\pi. \tag{56}$$

Again, since wideband ideal phase shifters are used in the linear antenna array, by substituting $\beta = \pi \cos\theta_m$ into (56), we have

$$kd\cos\theta - \pi\cos\theta_m > -2\pi, \tag{57}$$

and after replacing $kd = \pi f_i/f_c$ into (57), we get

$$\cos\theta > \frac{\cos\theta_m - 2}{f_i} f_c. \tag{58}$$

As $\cos\theta > -1$, we have $\frac{\cos\theta_m - 2}{f_i} f_c < -1$ based on (58), which also yields (55).

If there exists only one grating lobe, replacing the inequality sign in (56) with an equal sign and substituting $\beta = kd\cos\theta_{mi}$ yields

$$\begin{aligned} \theta_{gi} &= \arccos\left(\frac{\beta}{kd} - \frac{2\pi}{kd}\right) \\ &= \arccos\left(\cos\theta_{mi} - \frac{c}{f_i d}\right). \end{aligned} \tag{59}$$

Substituting (53) into (52) reveals that when $f_i \in [(2 - \cos\theta_m) f_c,\ (2 + \cos\theta_m) f_c)$, this wideband linear array will have only one grating lobe at the operating frequency f_i in the direction of θ_{gi}.

Appendix 2. Feasible domain for two-user PD-NOMA pairing at a given SIC decoding power ratio constraint

The existing approach of allocating transmit power by a strategy of maximizing the minimum rate among NOMA users [17] does not maximize the sum rate of NOMA user pairs. The beam design problem when maximizing the sum rate of a two-user NOMA pair is considered in [13]. In contrast, because of the employment of frequency squint beams, the problem of power allocation to NOMA users under a steering beam and the matching of NOMA pairs due to SIC decoding power constraints are mainly addressed in this subsection.

The power allocation problem to maximize the sum rate of paired NOMA user groups can be generally described as

$$\begin{aligned} &\max_{\beta_i\ i\in\{1,2,\cdots,N\}} \sum_i R_i, \\ &\quad s.t. \quad \sum_{j=1}^{N} \beta_j \le 1, \\ &\qquad 0 \le \beta_j, \quad for\, j \in \{1, 2, \cdots, N\}, \end{aligned} \tag{60}$$

where $\{1, 2, \cdots, N\}$ is the set of users in the NOMA pair, R_i is the rate of the i^{th} user, and β_i is the proportion of transmit power allocated to that user's signal at the BS side. Firstly, it is necessary to select the appropriate NOMA pair such that the channel quality differs significantly across users. Secondly, the power allocation strategy of the NOMA pair is to maximize the rate of the users with good channel quality while guaranteeing the minimum QoS requirements of the users with poor channel quality. If it is not possible to simultaneously serve the users in the pair to guarantee their QoS, then the lower priority users in the NOMA group are dropped or the users with good channel conditions are served.

In a two-user NOMA pairing scheme in which the BS side and the subscriber end are equipped with a single-antenna scenario, it is assumed without loss of generality that the channel quality of user 2 is better than that of user 1, i.e., $|h_1|^2 < |h_2|^2$, and this optimization problem is equivalent to satisfying the minimum rate requirement t_1 for the far user with poor channel quality to maximize the rate of the near user with a better channel condition, that is

$$\begin{aligned} &\max_{\beta_i\ i\in\{1,2\}} R_2, \\ &s.t. \quad \beta_1+\beta_2 \le 1, \\ &\qquad R_1 = t_1, \\ &\qquad 0 \le \beta_1, \\ &\qquad 0 \le \beta_2, \end{aligned} \tag{61}$$

This problem has been solved, and according to the work in [17], it follows that

$$\beta_1 = \frac{2^{t_1}-1}{P|h_1|^2}\left(P|h_1|^2\beta_2+\sigma_n^2\right). \tag{62}$$

Substituting $\beta_2 = 1-\beta_1$ into (62), we get

$$\beta_1 = \frac{\left(2^{t_1}-1\right)\left(P|h_1|^2+\sigma_n^2\right)}{2^{t_1}P|h_1|^2}, \tag{63}$$

$$\beta_2 = \frac{P|h_1|^2-\left(2^{t_1}-1\right)\sigma_n^2}{2^{t_1}P|h_1|^2}. \tag{64}$$

The power allocation coefficient for user 2 in the pair needs to satisfy

$$0 < \beta_2 \le \beta_2^{\max}, \tag{65}$$

where the left inequality is due to the fact that the effective power distribution needs to be positive and the right inequality is a restriction on the proportion of power that can be successfully decoded by the SIC; substituting these two constraints into (64) respectively gives

$$P|h_1|^2-\left(2^{t_1}-1\right)\sigma_n^2 > 0, \tag{66}$$

$$\left(1-\beta_2^{\max}2^{t_1}\right)|h_1|^2 \le \left(2^{t_1}-1\right)\sigma_n^2/P. \tag{67}$$

- When $1-\beta_2^{\max}2^{t_1} \le 0$, since the left side of the inequality in (67) is non-positive, (67) holds constant, it follows that

  $$\beta_2^{\max} \ge 2^{-t_1}. \tag{68}$$

  It means that the constraint imposed by the right-hand inequality in (65) vanishes as long as (68) is satisfied.
- When $1-\beta_2^{\max}2^{t_1} > 0$, it follows from (67) that

  $$|h_1|^2 \le \frac{2^{t_1}-1}{1-\beta_2^{\max}2^{t_1}}\cdot\frac{\sigma_n^2}{P}. \tag{69}$$

If this NOMA pair matches, then there is

$$R_1 = t_1, \tag{70}$$

$$R_2 = \log_2\left(1+2^{-t_1}|h_2|^2\left(\frac{P}{\sigma_n^2}-\frac{2^{t_1}-1}{|h_1|^2}\right)\right). \tag{71}$$

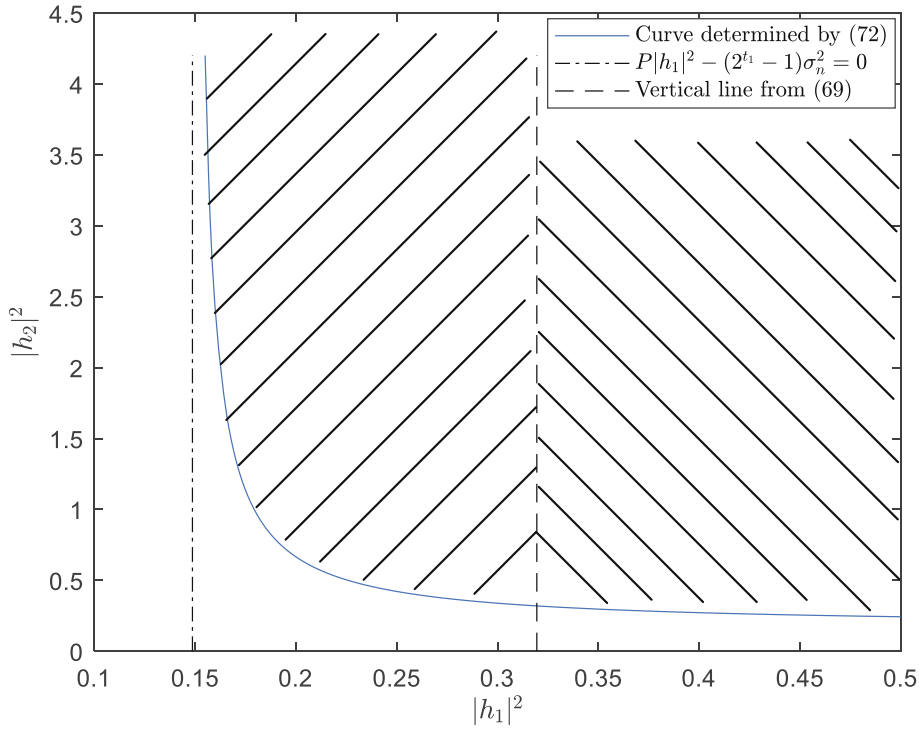

Fig. 8 The NOMA feasible domain, with $t_1 = t_2 = 0.2$ and $P/\sigma_n^2 = 1$, as an example

As can be seen when the NOMA pair is matched, the worse the channel quality of user 1, the smaller the rate of user 2; the better the channel quality of user 2, the larger the rate of user 2.

Let the minimum rate requirement for user 2 be t_2, i. e., $R_2 \geq t_2$ needs to be satisfied; substituting (71), we have

$$\frac{2^{t_1} - 1}{|h_1|^2} + \frac{2^{t_1}\left(2^{t_2} - 1\right)}{|h_2|^2} \leq \frac{P}{\sigma_n^2}. \tag{72}$$

Figure 8 shows the feasible domain of the channel state for the two-user PD-NOMA pair in (72), illustrated by $t_1 = t_2 = 0.2$ and $P/\sigma_n^2 = 1$, where the curved part is one of the hyperbolas determined in (72), the vertical dashed line on the left is determined by the left inequality in (65), and the vertical dashed line on the right is set according to the SIC decoding requirements and determined by the right inequality in (65). When (68) holds, the entire shaded region is the NOMA feasible domain, whereas when (68) is not satisfied, the shaded region on the left is the feasible domain of the actual matched pair.

Abbreviations

PD-NOMA: Power-domain non-orthogonal multiple access; BS: Base station; SIC: Successive interference cancellation; mmWave: Millimeter-wave; RF: Radio frequency; AoD: Angle-of-departure; JSDM: Joint spatial division and multiplexing; HPBW: Half-power beamwidth; PU: Primary user; SU: Secondary user

Acknowledgements

Not applicable.

Authors' contributions

XP contributed with the research idea, methods, and simulations and was a major contributor in writing the manuscript. LY further examined the manuscript and corrected it. All authors read and approved the final manuscript.

Funding
This work was supported in part by the National Key R&D Program of China under Grant 2020YFB1804901, in part by the National Natural Science Foundation of China under Grants 61971128 and U1936201.

Availability of data and materials
Data sharing is not applicable to this article as no datasets were generated or analyzed during the current study.

Declarations

Competing interests
The authors declare that they have no competing interests.

Received: 27 April 2021 Accepted: 12 July 2021
Published online: 06 August 2021

References

1. S. K. Garakoui, E. A. M. Klumperink, B. Nauta, F. E. van Vliet, in *2011 41st European Microwave Conference*, Phased-array antenna beam squinting related to frequency dependency of delay circuits, (2011), pp. 1304–1307. https://doi.org/10.23919/EuMC.2011.6101846
2. S. K. Garakoui, E. A. M. Klumperink, B. Nauta, F. E. van Vliet, in *Proceedings of 2010 IEEE International Symposium on Circuits and Systems*, Time delay circuits: a quality criterion for delay variations versus frequency, (2010), pp. 4281–4284. https://doi.org/10.1109/ISCAS.2010.5537554
3. X. Pan, C. Li, M. Hua, W. Yan, L. Yang, Compact multi-wideband array for millimeter-wave communications using squint beams. IEEE Access. **8**, 183146–183164 (2020). https://doi.org/10.1109/ACCESS.2020.3027835
4. O. E. Ayach, S. Rajagopal, S. Abu-Surra, Z. Pi, R. W. Heath, Spatially sparse precoding in millimeter wave MIMO systems. IEEE Trans. Wirel. Commun. **13**(3), 1499–1513 (2014). https://doi.org/10.1109/TWC.2014.011714.130846
5. A. A. Saleh, R. Valenzuela, A statistical model for indoor multipath propagation. IEEE J. Sel. Areas Commun. **5**(2), 128–137 (1987)
6. C. A. Balanis, *Antenna Theory: Analysis and Design*. (Wiley, Hoboken, 2016)
7. A. Adhikary, J. Nam, J. Ahn, G. Caire, Joint spatial division and multiplexing–the large-scale array regime. IEEE Trans. Inf. Theory. **59**(10), 6441–6463 (2013). https://doi.org/10.1109/TIT.2013.2269476
8. A. Adhikary, E. Al Safadi, M. K. Samimi, R. Wang, G. Caire, T. S. Rappaport, A. F. Molisch, Joint spatial division and multiplexing for mm-wave channels. IEEE J. Sel. Areas Commun. **32**(6), 1239–1255 (2014). https://doi.org/10.1109/JSAC.2014.2328173
9. S. M. R. Islam, N. Avazov, O. A. Dobre, K. Kwak, Power-domain non-orthogonal multiple access (NOMA) in 5G systems: potentials and challenges. IEEE Commun. Surv. Tutor. **19**(2), 721–742 (2017)
10. Z. Ding, X. Lei, G. K. Karagiannidis, R. Schober, J. Yuan, V. K. Bhargava, A survey on non-orthogonal multiple access for 5G networks: research challenges and future trends. IEEE J. Sel. Areas Commun. **35**(10), 2181–2195 (2017). https://doi.org/10.1109/JSAC.2017.2725519
11. L. Dai, B. Wang, Z. Ding, Z. Wang, S. Chen, L. Hanzo, A survey of non-orthogonal multiple access for 5G. IEEE Commun. Surv. Tutor. **20**(3), 2294–2323 (2018)
12. Z. Wei, L. Zhao, J. Guo, D. W. K. Ng, J. Yuan, Multi-beam NOMA for hybrid mmWave systems. IEEE Transactions on Communications. **67**(2), 1705–1719 (2019). https://doi.org/10.1109/TCOMM.2018.2879930
13. Z. Xiao, L. Zhu, J. Choi, P. Xia, X. Xia, Joint power allocation and beamforming for non-orthogonal multiple access (NOMA) in 5G millimeter wave communications. IEEE Trans. Wirel. Commun. **17**(5), 2961–2974 (2018). https://doi.org/10.1109/TWC.2018.2804953
14. C. Li, H. J. Yang, F. Sun, J. M. Cioffi, L. Yang, Multiuser overhearing for cooperative two-way multiantenna relays. IEEE Trans. Veh. Technol. **65**(5), 3796–3802 (2016). https://doi.org/10.1109/TVT.2015.2441879
15. C. Li, P. Liu, C. Zou, F. Sun, J. M. Cioffi, L. Yang, Spectral-efficient cellular communications with coexistent one- and two-hop transmissions. IEEE Trans. Veh. Technol. **65**(8), 6765–6772 (2016). https://doi.org/10.1109/TVT.2015.2472456
16. C. Li, J. Wang, F.-C. Zheng, J. M. Cioffi, L. Yang, Overhearing-Based Co-Operation for Two-Cell Network With Asymmetric Uplink-Downlink Traffics. IEEE Trans. Signal Inf. Process Over Netw. **2**(3), 350–361 (2016). https://doi.org/10.1109/TSIPN.2016.2549179
17. S. Timotheou, I. Krikidis, Fairness for non-orthogonal multiple access in 5G systems. IEEE Signal Process. Lett. **22**(10), 1647–1651 (2015). https://doi.org/10.1109/LSP.2015.2417119

Publisher's Note